行政院國家科學委員會專題研究計畫　成果報告

新型表面擇頻元件之設計：分析與計算

計畫類別：個別型計畫
計畫編號：NSC93-2212-E-002-080-
執行期間：93 年 10 月 01 日至 94 年 07 月 31 日
執行單位：國立臺灣大學應用力學研究所

計畫主持人：陳瑞琳

計畫參與人員：洪士哲,楊適壕

報告類型：精簡報告

處理方式：本計畫可公開查詢

中　華　民　國 94 年 10 月 28 日

ABSTRACT

Because of the filtering property suggested, two-dimensional periodic screens which were named the frequency selective surfaces (FSS) have attracted a great deal of attention for many years and have been found various applications, such as band-pass radomes, reflectors of antenna system, polarizers and so on. The frequency response of FSS highly depends on the configurations and spacing of the elements as well as on the thickness and permittivity of dielectric layers that may be part of the screens.

When an incident field propagates through FSS, surface currents will be induced on the conducting screens and then, in turn, radiate a scattered field. In this thesis, we employ the spectral Galerkin method to analyze the scattering phenomena of the FSS. In the spectral domain, Floquet's theorem allows the induced surface currents to be expressed in terms of a Fourier series and reduces the computation domain from an infinite array into a single cell. For the FSS with multilayered structures, we also employ the spectral immitance approach to derive the spectral dyadic Green's functions which relate the induced surface currents to the scattered field.

Moreover, to be more feasible for analyzing FSS with complex configurations, the subdomain basis functions are adopted to expand the induced currents. Although that will increase the number of unknowns, the computation speed can be improved by using a fast Fourier transform based iterative approach (the conjugate gradient method, FFTCG). After the distribution of the induced surface currents is determined, the spectral scattered fields can be found. Finally, we can express the reflection and transmission coefficients at different Floquet modes in terms of the spectral scattered fields at the top and bottom surfaces of the FSS.

Results for the free-standing and the single-layered-dielectric FSS with various geometries are presented, and are compared with existing results to check the correctness of our programming. In addition, some parameters, such as the configurations of the conducting screens, the thickness and the permittivity of the dielectric layers, which describe the structure of the FSS are varied to investigate the resultant effects on the frequency response.

摘　要

「頻率選擇表面」（frequency selective surfaces）是由一群在空間中呈週期性排列的金屬所組成的二維陣列。由於其濾波的特性，多年來，吸引了大量研究工作的投入。研究中發現，頻率選擇平面在電磁波的許多頻段中，具有廣泛的應用。例如在微波中可用於雷達或天線系統，在紅外光的頻段中則可用於極化器或提升分子雷射的效率。能夠影響頻率選擇表面之頻率響應的因素有許多，諸如金屬排列的幾何形狀、週期長度及其間隙大小；而作為其基底之介電材料的電磁特性及厚度也是需要考量的因素。

當入射波通過頻率選擇表面時會在金屬的表面誘發出表面電流，進而由這些表面電流激發出散射場。在本文中，我們採用頻率域的 Galerkin 方法來分析有關頻率選擇表面散射場的問題。在頻率域裡，我們引進 Floquet 理論，使得誘發表面電流能以傅立葉級數的形式來表示，而計算域也從無限延伸的陣列減少至單一週期。在建立散射場和誘發表面電流的關係式後，帶入金屬表面的邊界條件，就可針對誘發表面電流求解。對於含有介電材料或多層結構的頻率選擇表面，則必須先採用 Itoh 所提出的頻域阻抗法（spectral domain immitance approach），以求得用來聯繫表面電流和散射場的 Green 函數，然後再進行求解。

為了方便分析幾何排列較為複雜的結構，我們採用小區域（subdomain）的基底函數將作為未知數的誘發表面電流展開。依循 Galerkin 法的步驟便可求得電流的分佈情形。當未知數的數目很大時，可仰賴適當的疊代法（本文採用共軛梯度法 conjugate gradient method），並配合快速傅立葉的運算法來提高求解的效率。根據誘發表面電流的分佈情形，位於整個頻率選擇表面結構之上表面及下表面的散射場即可以頻域的形式求得。最後，在不同 Floquet 模態下的反射和穿透係數，皆可由這些位於上、下表面的散射場來表示，對於頻率選擇表面之頻率響應的分析就完成了。

本文針對不同結構的頻率選擇表面，分析其於不同極化方向的入射波在不同角度入射下所對應的頻率響應，並與已知的結果作比對，來驗證理論和計算過程的正確性。之後再改變用來描述頻率選擇表面結構的參數，如介電值的厚度、介電常數或金屬排列的方式，以觀察其對於頻率響應的影響。

1 Introduction

Two-dimensional planar periodic structures with frequency filtering property are named "frequency selective surfaces" (FSS). Generally, the structures of FSS consist of conducting patch elements or aperture elements within a metallic screen periodically arranged in the space as shown in Fig. 1-1(Wu, 1995), and are printed on a substrate or sandwiched between dielectrics. For a lossless structure, there exists a single frequency at which an FSS allows the incident fields either totally transmitting or totally reflecting; in the neighborhood of that frequency, a pass-band or a stop-band will form. This frequency as well as the band depends upon some parameters: the configurations of the patch or aperture elements, element spacing, thickness and permittivity of any dielectric layers, and the polarization of the incident fields (Cwik and Mittra, 1987). On one hand, these parameters provide the degrees of design freedom to meet our needs, and, on the other hand, increase the complexity of the physical phenomena to be observed.

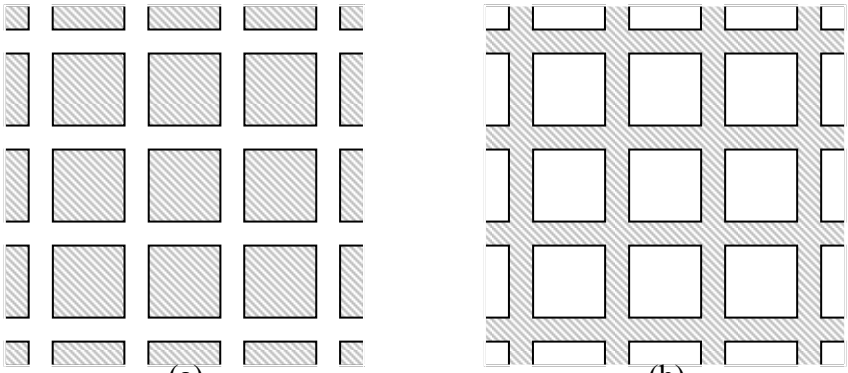

FIGURE 1-1 Frequency selective surfaces with periodically arranged (a) conducting patch elements and (b) aperture elements within a metallic screen (the shaded regions typify the portions of metal).

The application of the FSS ranges over much of the electromagnetic spectrum. In the microwave region, the FSS are used as band-pass radomes (Lee, 1971) and as subreflectors of the dual frequency reflector antenna systems (Mittra, Chan and Cwik, 1988). In the far-infrared and submillimeter wave region, the FSS are used as polarizers, beam splitters, and cavity couplers for improving the pumping efficiency in molecular lasers (Ulrich, 1967; Durschlag and DeTemple, 1981). In the near-infrared spectrum, they are used as solar selective surfaces to aid in the collection of solar energy (Horwitz, 1974).Recently, the FSS are proposed to be 2-D artificial electromagnetic band-gap (EBG) or photonic band-gap (PBG) structures, to realize the conceptually perfect magnetic conductors (PMC) on which the transverse components of the magnetic fields vanish. (Monorchio, Manara and Lanuzza, 2002 and 2003; Junho, Mittra and Chakravarty, 2002).

In this thesis, we use the spectral domain method of moments to analysis the FSS, especially on the spectral domain Galerkin method in which the testing functions are chosen to be the same with the basis functions.equations as well as the method of moments (MoM) for solving integral equations.

2 Theory

2.1 Problems

When an incident wave propagates through the FSS, it will induce some surface currents on the conducting screens which will, in turn, radiate the scattered field. Then the total (resultant) field in the free space is the sum of the incident field and the scattered field (Fig. 2-1).

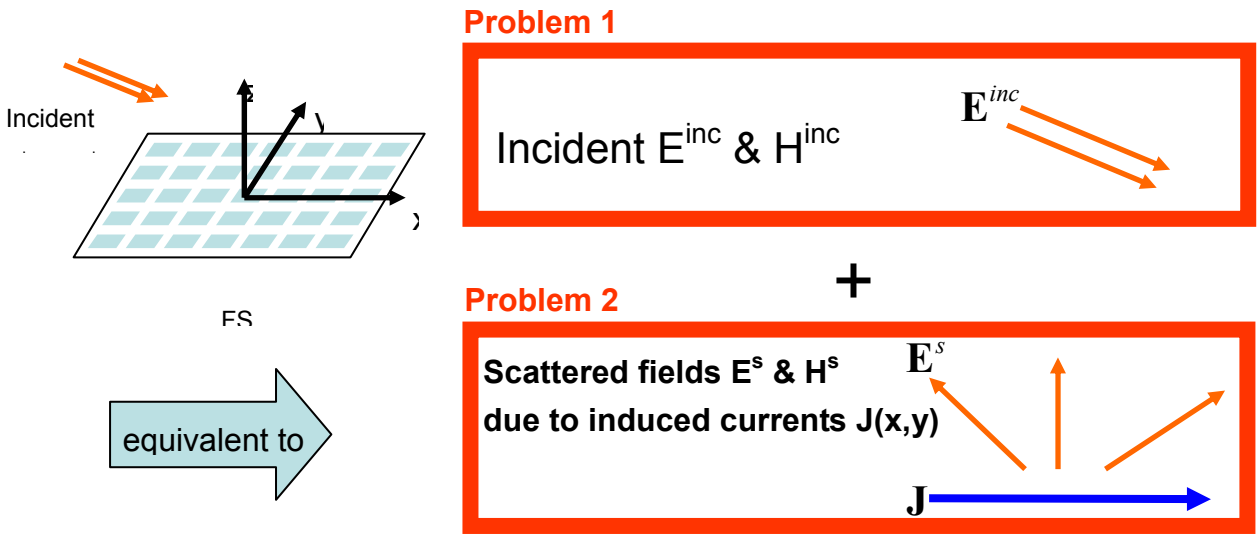

FIGURE 2-1 $\mathbf{E}^{total} = \mathbf{E}^{inc} + \mathbf{E}^{s}$

2.2 Assumptions

Several assumptions are declared here:

1. The FSS is infinitely extended so that the diffraction from the edges of the surface in a practical situation can be ignored.
2. The incident radiation is a monochromatic plane wave (other sources can be treated as a superposition of plane waves).
3. The conducting screen is infinitesimally thin.

When an incident wave propagates through the FSS, it will induce some surface currents on the conducting screens which will, in turn, radiate the scattered field. Then the total (resultant) field in the free space is the sum of the incident field and the scattered field (Fig. 2-1).

2.3 Scattered Field for single FSS

From Maxwell's equations

$$\nabla \times \mathbf{E}^{s} = -j\omega\mu_0 \mathbf{H}^{s}$$

$$\nabla \times \mathbf{H}^{s} = j\omega\varepsilon_0 \mathbf{E}^{s} + \mathbf{J}$$

$$\nabla \bullet \mathbf{E}^{s} = \rho/\varepsilon_0$$

$$\nabla \bullet \mathbf{H}^{s} = 0$$

Then the governing equation is

$$\nabla^2 \mathbf{A} + k_0^2 \mathbf{A} = -\mathbf{J}$$

where $\mathbf{A}$ is vector potential.

We can express $\mathbf{E}^s$ in terms of $\mathbf{A}$ as

$$\mathbf{E}^s = -j\omega\mu_0\mathbf{A} + \frac{1}{j\omega\varepsilon_0}\nabla\left(\nabla\bullet\mathbf{A}\right)$$

The solution of is

$$\mathbf{A} = G * \mathbf{J} = \int G\left(\mathbf{r},\mathbf{r}'\right)\mathbf{J}\left(\mathbf{r}'\right)d\mathbf{r}'$$

where

$$G\left(\mathbf{r},\mathbf{r}'\right) = \frac{e^{-jk_0|\mathbf{r}-\mathbf{r}'|}}{4\pi|\mathbf{r}-\mathbf{r}'|}$$

Since the periodicity of FSS, we apply Floquet's theorem for induced surface current. Thus the scarttered field can be written as

$$\begin{bmatrix} E_x^s\left(x,y\right) \\ E_y^s\left(x,y\right) \end{bmatrix} = \frac{1}{j\omega\varepsilon_0}\sum_{m=-\infty}^{\infty}\sum_{n=-\infty}^{\infty}\begin{bmatrix} k_0^2-\alpha_m^2 & -\alpha_m\beta_n \\ -\alpha_m\beta_n & k_0^2-\beta_n^2 \end{bmatrix}\times\tilde{G}\left(\alpha_m,\beta_n\right)\begin{bmatrix} \tilde{J}_x\left(\alpha_m,\beta_n\right) \\ \tilde{J}_y\left(\alpha_m,\beta_n\right) \end{bmatrix}e^{j\alpha_m x}e^{j\beta_n y}$$

When the conductivity of the patch is finite, the boundary condition must be modified to the impedance boundary condition (Mittra et al., 1988, Eq. 10):

$$\begin{bmatrix} E_x^{inc} \\ E_y^{inc} \end{bmatrix} + \begin{bmatrix} E_x^s \\ E_y^s \end{bmatrix} = R_s\begin{bmatrix} J_x \\ J_y \end{bmatrix}$$

In practical applications of interest, the FSS may be printed on a substrate, embedded between dielectric layers together with a supporting dielectric substrate and/or superstrate. The FSS may even be structured as multiple screens for additional degrees of design freedom. Thus, for a multilayered FSS with *M* conducting screens (Fig. 2-4), the induced currents on each of the conducting surfaces are related to the scattered fields or the incident fields by

$$-\begin{bmatrix} E_{ix}^{inc} \\ E_{iy}^{inc} \end{bmatrix} = \sum_{j=1}^{M}\sum_{-\infty}^{\infty}\sum_{-\infty}^{\infty}\begin{bmatrix} \tilde{G}_{xx}^{ij} & \tilde{G}_{xy}^{ij} \\ \tilde{G}_{yx}^{ij} & \tilde{G}_{yy}^{ij} \end{bmatrix}\begin{bmatrix} \tilde{J}_{jx} \\ \tilde{J}_{jy} \end{bmatrix}e^{j(\alpha_m x+\beta_n y)} - R_s\begin{bmatrix} J_{ix} \\ J_{iy} \end{bmatrix}$$

Where $i = 1, 2\ldots M$. The subscript *i* corresponds to the *i*th conducting surface, and the left-hand side corresponds to the sum of the scattered fields due to the current on each of the *j* surfaces

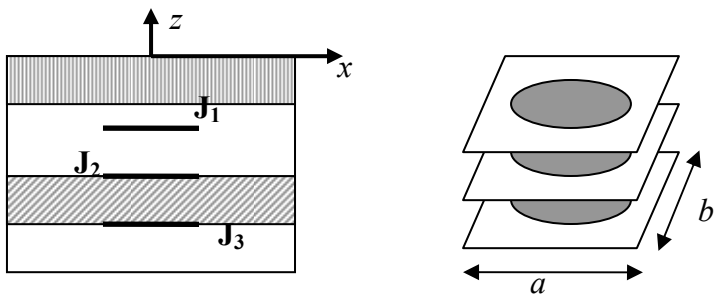

FIGURE 2-2 Multilayered FSS (ref. from Chan, 1995, pp. 49).

The spectral dyadic Green's function is calculated in the presence of the dielectric layers by using the spectral domain immitance approach which was presented by Itoh (1980).

2.4 Numerical Method: Method of Moment

The procedure to analyze the scattering problems of the frequency selective surfaces is: first,

determine the distributions of the induced currents by means of the spectral domain Galerkin method; second, calculate the scattered fields at the top and the bottom surfaces of the whole structure of the FSS; finally, expressing the reflection and transmission coefficients at different Floquet modes in terms of the total reflected and transmitted fields in the spectral domain.

The unknown surface current $\mathbf{J}$ can be express by basis functions which is roof-top functions (Figure 2-3) as

$$\mathbf{E}^{inc} = \mathbf{LJ}$$

where $\mathbf{L}$ is the operator relating $\mathbf{E}^{inc}$ and $\mathbf{J}$.

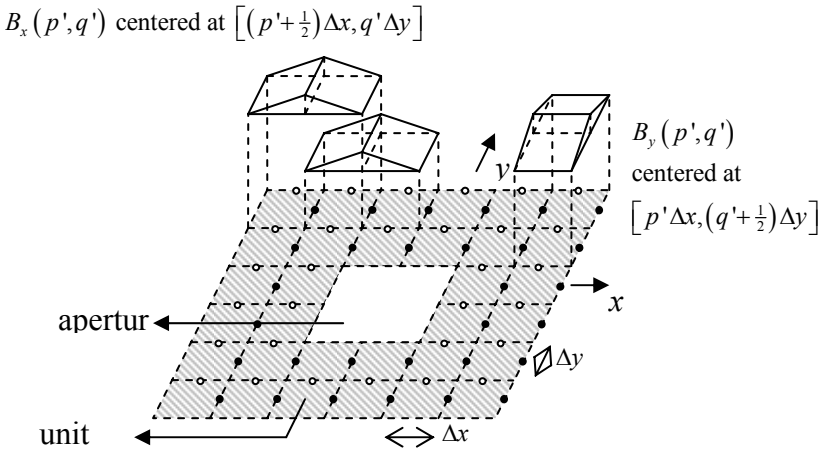

FIGURE 2-3 *x*-directed and *y*-directed roof-top basis functions

Applying Galerkin method choosing the test functions same with basis functions and using fast Fourier transform for time consuming. Finally, we use the conjugate gradient method to solve the amplitudes of surface currents.

3 Numerical Results and Discussion

We present several results from calculations. Some typical cases, such as square patch, Jerusalem cross and slot aperture, are presented and compared with the existing results for verifying the correctness of the computations. Then, some modifications for the configurations and the permittivity of the dielectric are made to change the characteristics of frequency response.

3.1 Square Plates

Consider a periodic array of lossless square plates (Rubin and Bertoni, 1983). The size of square plates is shown in Figure 3-1. It is illuminated by a normally incident field. The electric field is polarized in the *x* direction and has a magnitude of 120πV/cm. We divide the unit cell into 16 × 16 grids. The distributions of the induced surface currents are plotted in Figure 3-2.

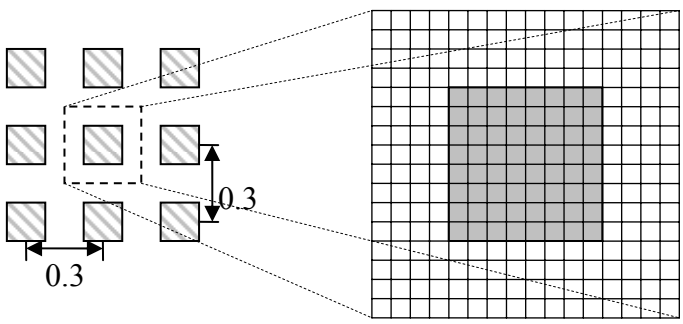

FIGURE 3-1 Periodic array of square plates.

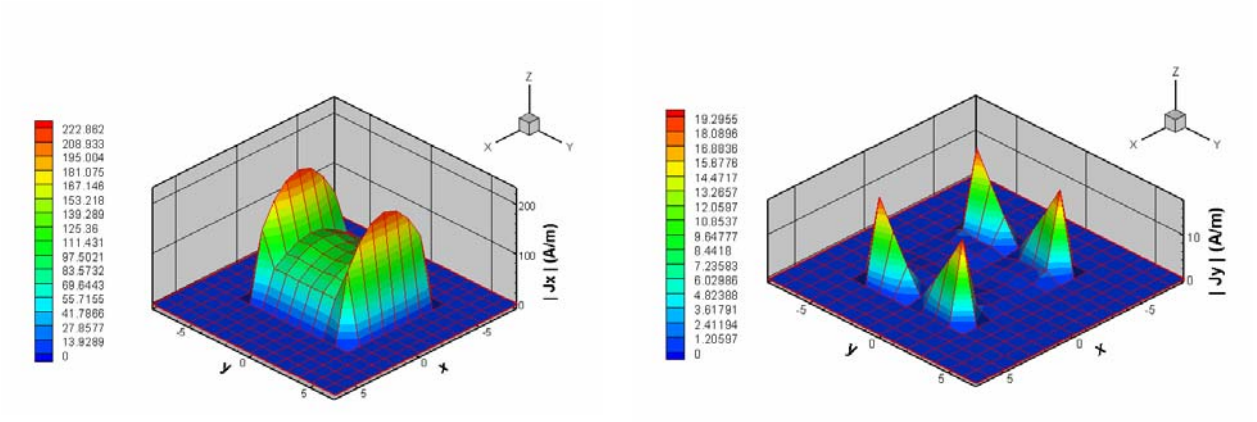

FIGURE 3-2 Distributions of the induced surface currents for the periodic array of square plates in x and y directions, respectively.

3.2 Thin Patches

Consider the thin conducting patch array described in Chen 1970. The size of each patch is shown in Fiqure 3-3. The analyses there were divided into two parts. The first part is that the incident angle was fixed to be normal to the conducting patches while the frequency changed. The second part is that the frequency of the incident field was fixed with different incident planes. We follow the procedures with a little modification and describe them in the following two subsections.

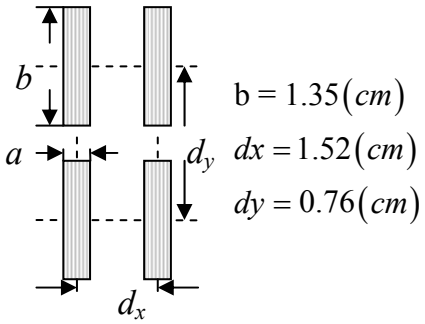

FIGURE 3-3 Periodic array of thin conducting patches.

3.2.1 Normal Incidence with Different a

In the first part, the array is illuminated by the normally incident waves polarized in *y* direction. The frequency ranges from 6GHz to 22GHz and the width of the patches is changed to be twofold and fourfold to investigate the resultant effects on the frequency response.In our calculation, we set the width *a* to be 0.1425cm, 0.2375cm and 0.5225cm, respectively. We divide the unit cell into 16 × 16 grids and therefore there are 67, 121 and 283 unknowns in these three respective cases. The magnitude and phases of reflection coefficients is shown in Figure 3-4.

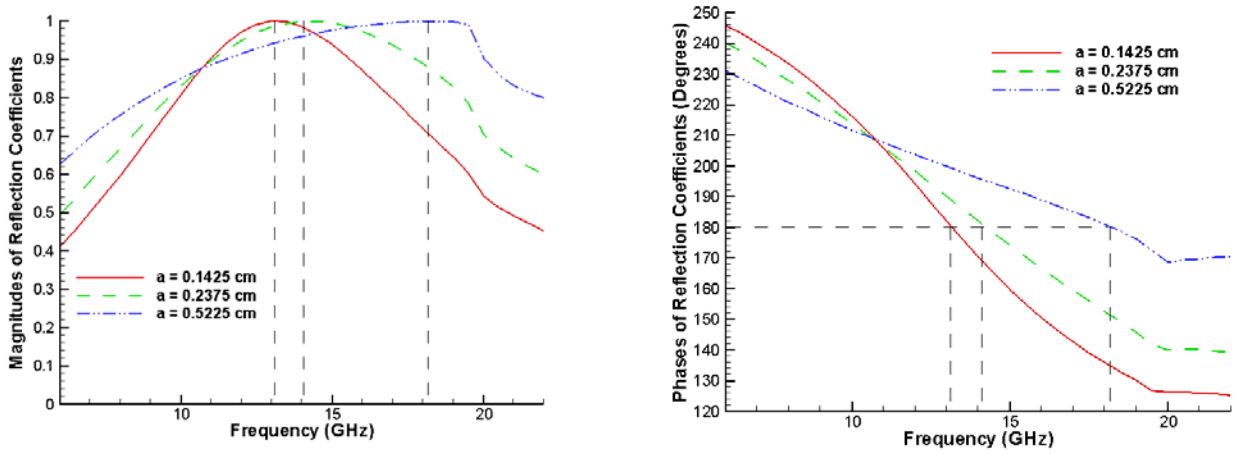

FIGURE 3-4 Periodic array of thin conducting patches.

The corresponding resonant frequencies where the total reflections occur are computed to be at 13.1GHz, 14.1GHz and 18.1GHz. It shows the fact that increasing the width of the patch will raise the resonant frequency. Moreover, the bandwidth also increases with the patch width. When the total reflections occur, the phases are about 180°.

3.2.2 Varying Incidence Angle

In this part, we consider the thin patch with size of $a \times b$ = 0.1425cm × 1.35cm. The frequency of the incident wave is fixed to be 13.1GHz at which the resonance occurred in the previous case. We vary the incident plane by setting φ = 0°, 30°, 45°, 60° and 90°, respectively. And the angle of incidence θ ranges from 0° to 90°. Both TE_z and TM_z polarized incident waves are considered. The results of TEz and TMz are as shown in Figure 3-5.

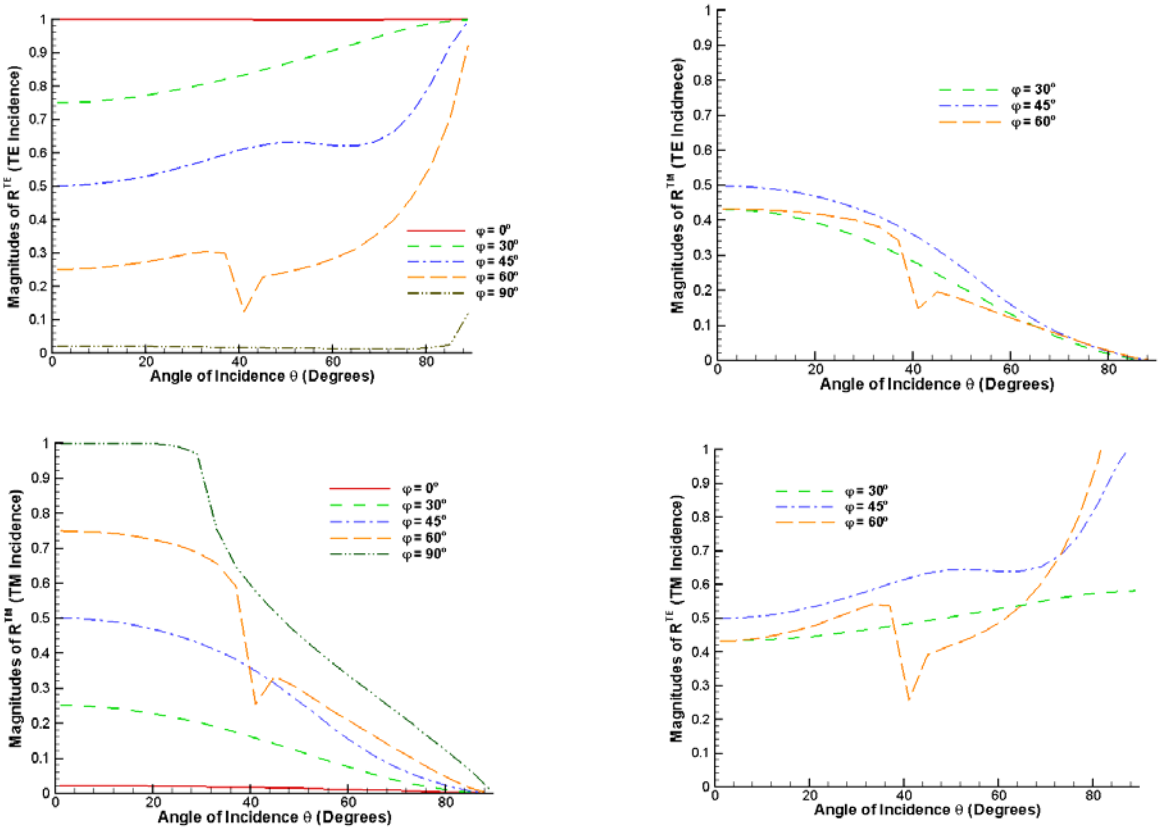

FIGURE 3-5 TE_z and TMz reflection coefficients of TEz and TM_z incidence.

Consistent to those calculated from Chen 1970, when θ = 0°, the incident wave is totally

reflected; when $\theta = 90^{o}$, the wave is totally transmitted. When the plane of incidence is the plane of $\varphi = 0^{o}$, the TM_z part of the reflected field for TE_z incidence and the TE_z part of the reflected field for TM_z incidence nearly vanish.

3.3 Slot Apertures

In this section, we consider the slot aperture FSS in several different situations (Mittra, Chan and Cwik, 1988). Some parameters, such as the dielectric constant of the substrate, thickness of the dielectric layer, and the way by which the configuration of the FSS is arranged, are modified to investigate the resultant effects on the frequency response.

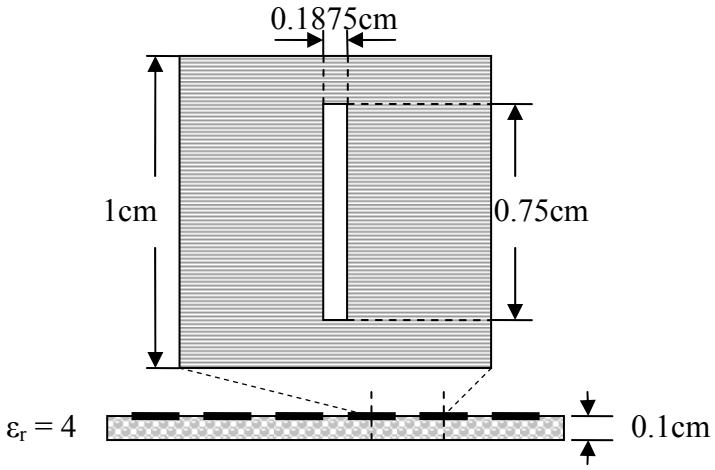

FIGURE 5-6 Slot aperture FSS with dielectric backing (Mittra et al., 1988).

3.3.1 Varying Dielectric Constants

The comparisons of the reflection coefficients among different dielectric constants under the illuminations of the incident waves propagating from different directions are presented in Figure 3-7. We find that when the dielectric constant increases, the resonant frequency becomes smaller. The pass-band is shifted toward left direction and, especially, the nearly total reflection region at low frequency is significantly narrowed as the dielectric constant increases.

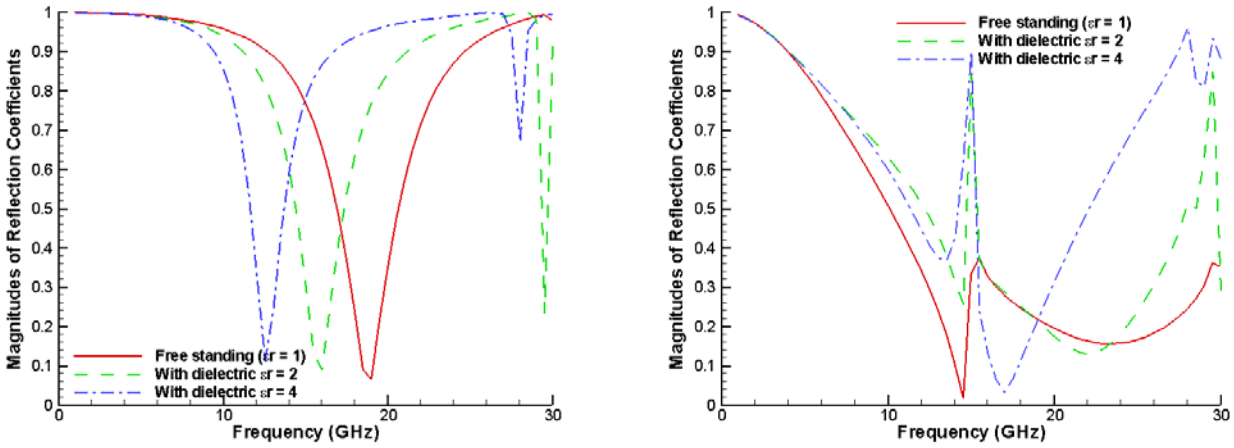

FIGURE 3-7 Comparison of reflection coefficients for $\theta = 0^{o}$ and $\theta = 80^{o}$ with the dielectric constant varying.

3.3.2 Varying Thickness of Dielectrics

We find that as the dielectric layer is thickened, the resonant frequency shifts toward left direction, and there are several higher resonances appearing as shown in Figure 3-8.

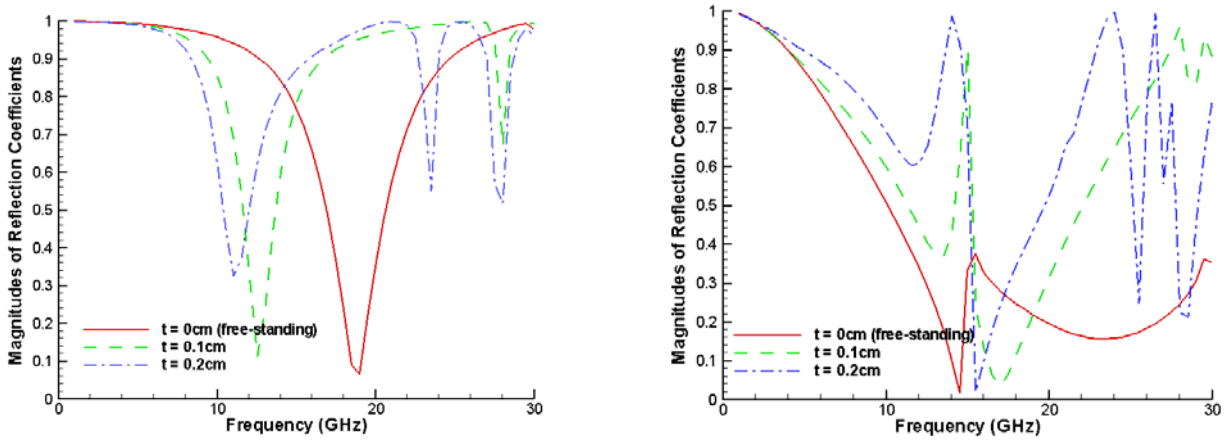

FIGURE 3-8 Comparison of reflection coefficients for $\theta = 0^o$ and $\theta = 80^o$ with the thickness of dielectric varying.

3.3.3 Fanned-Out Slot Apertures

We rearrange the configuration of the original slot aperture array in a fanned-out fashion (Figure 3-9).

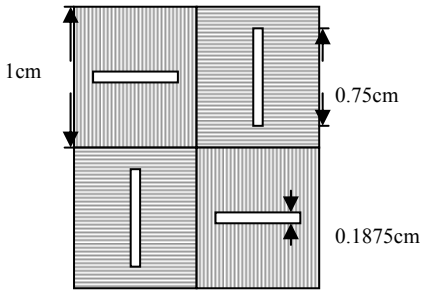

FIGURE 3-9 Slot apertures arranged in a fanned-out fashion.

From our computations, it is seen that the fanned-out arrangement narrows the pass-bands and shifts the resonant frequency to left. The nearly total reflection regions at low frequency are widened and the regions in which the structure turns to reach it first resonance are significantly reduced. The comparisons between these two different configurations are presented in Figure 3-10.

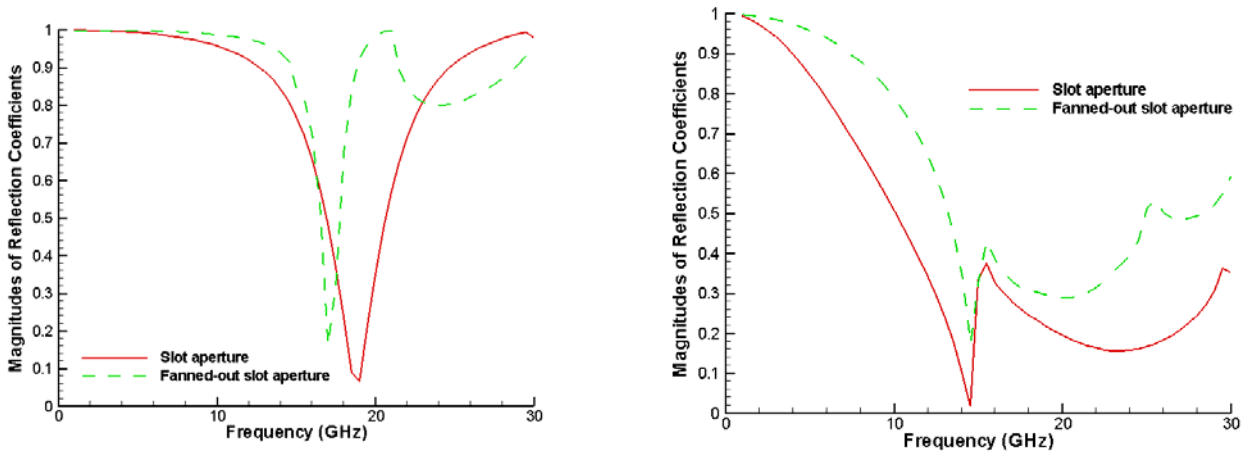

FIGURE 3-10 Comparison of reflection coefficients (θ=0^o, θ=80^o) for free-standing slot apertures of different configurations.

3.4 Jerusalem Crosses

There the free-standing arrays of conducting Jerusalem cross (Tsao and Mittra, 1984) patches with or without four additional cross dipoles are considered. Their geometries and sizes are depicted in Figure 3-9. The incident wave is polarized in the y direction. In our computations,

we divide the unit cell into 32 × 32 grids.

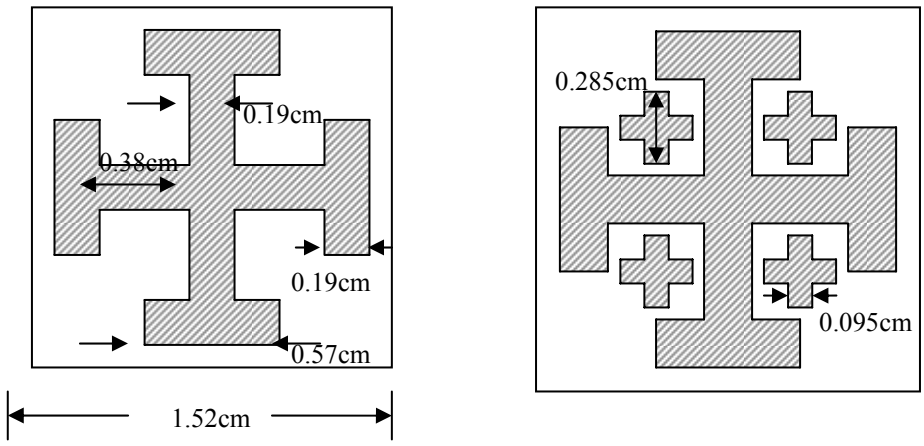

FIGURE 3-9 TE$_z$ and TMz reflection coefficients of TEz and TM$_z$ incidence.

From Figure 3-10 , we find that the resonant frequency is at 8 GHz.

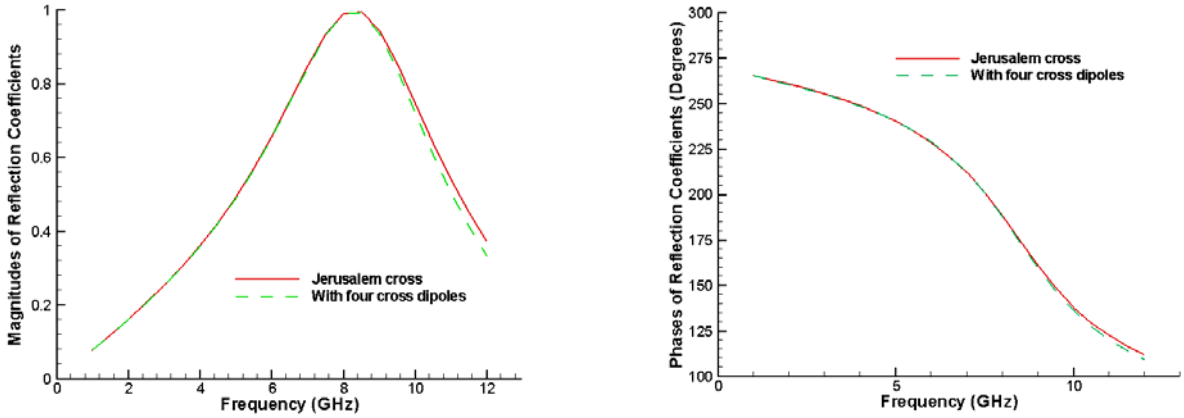

FIGURE 3-9 TE$_z$ and TMz reflection coefficients of TEz and TM$_z$ incidence.

3.5 Finite Conductivity

Consider the FSS with finite conductivity, thus the energy have dissipation. The geometry of the FSS and the reflection coefficients with different impedances are shown in Figure 3-10. The first resonance frequency is $T_x/\lambda = 0.92$. The power of reflection, transmission and dissipation coefficients at $T_x/\lambda = 0.92$ show in Figure 3-10.

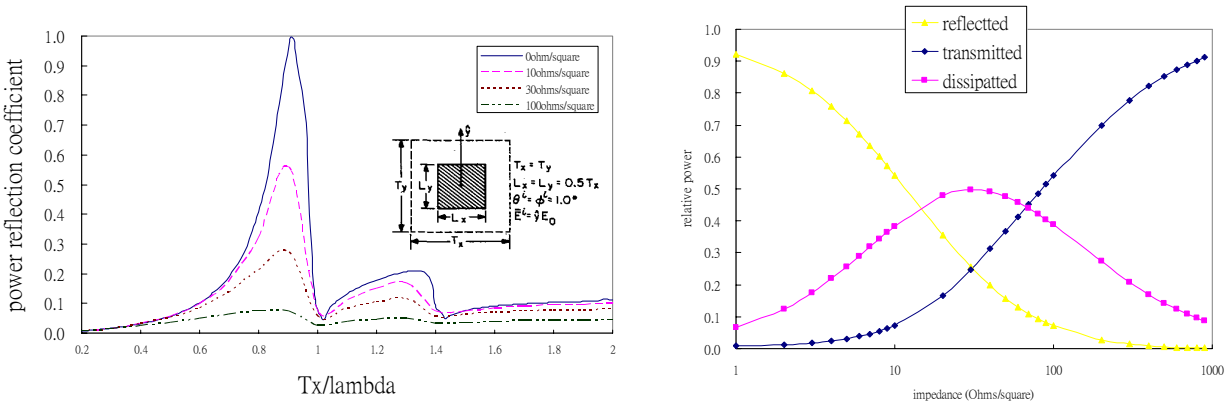

FIGURE 3-10 The FSS with finite conductivity

3.6 Multi-Screen FSS

Consider the patch-aperture-patch structure in Figure 3-11 (Chan, 1995). The transmitted

response is shown in Figure3-12. The results show that: 1.the response of TE and TM incidence have no significant difference. 2. the frequency of first resonance is between 10 and 11GHz, and the frequency of second resonance is between 14 and 16GHz. 3.low transmission occurs about 17 GHz.

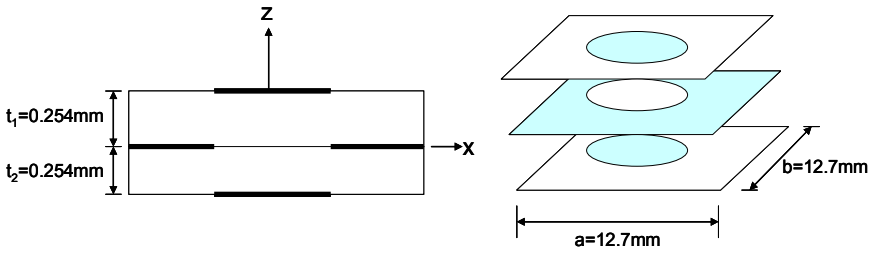

FIGURE 3-11 The multi-screen FSS

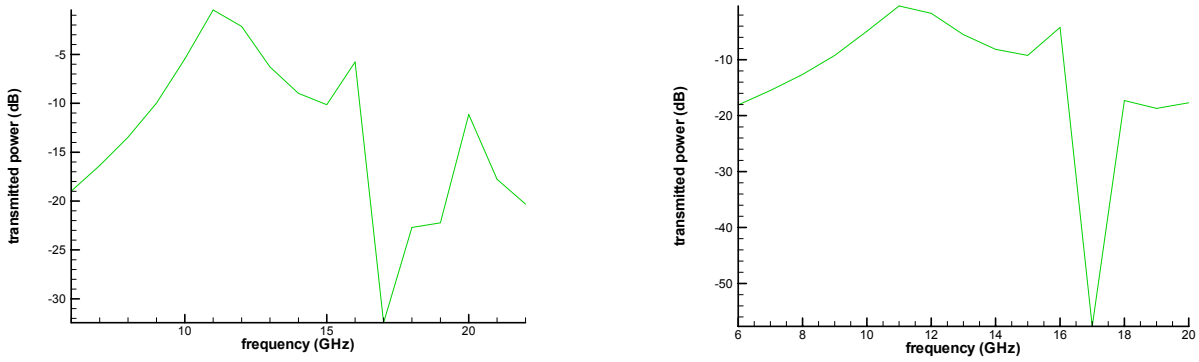

TE incidence TM incidence

FIGURE 3-11 The multi-screen FSS

4 Concluding Remarks

In this thesis, we studied how to analyze the scattering problems of frequency selective surfaces by using the spectral domain Galerkin medthod.

The exhaustive derivations have been given to establish the relations among the induced surface currents, scattered fields, and reflection and transmission coefficients.

The roof-top basis functions have been employed to expand the induced surfaced currents and could be utilized for arbitrarily complicated geometries. The fast Fourier transform algorithm and the conjugate gradient method indeed improve the efficiency of our computations when the number of unknowns was large. The spectral immitance approach was applied to find the spectral dyadic Green's functions for multilayered FSS.

We have analyzed several cases, such as square plates, thin conducting patches, Jerusalem cross with and without four additional cross dipoles, and slot apertures backed by a layer of dielectric.And in the case of the slot apertures, we change, in turn, the dielectric constants, thickness of the dielectric layer and the configurations, and found that the effects of shifting the resonant frequencies and narrowing the pass-bands were produced.

Because there are many factors, such as geometry and periodicity of the conducting screens, thickness and permittivity of the dielectrics, can influence the frequency response of the frequency selective surfaces, it provides us very high degrees of design freedom. However, it also

complicates the process of design since the effects of these factors usually couple to one the other. So, to precisely understand the physical properties of the individual factor is a very urgent task to us.

In addition, we expect that the scattering problems of FSS can be solved by being combined with some optimization algorithm, for example, the genetic algorithm, in the future. Thus, as inputting some particular demands, proper structures that meet the demands will be produced after the optimization, and the time consumed in the process of trial can be reduced.

5 Reference

Balanis, C. A. (1989) *Advanced Engineering Electromagnetics*, John Wiley & Sons, Inc, pp. 256-257.

Chan, C. H. (1995) "Analysis of frequency selective surfaces," in *Frequency Selective Surface and Grid Array, Wiley Series in Microwave and Optical Engineering*, T. K. Wu Ed., John Wiley & Sons, Inc, New York, pp. 27-86.

Chen, C. C. (1970) "Scattering by a two-dimensional periodic array of conducting plates," *IEEE Transactions on Antennas Propagation*, vol. 18, no. 5, pp. 660-665, Sep.

Cheng, D. K. (1989) *Field and Wave Electromagnetics*, Addison-Wesley Publishing Company, Inc., pp. 449-451.

Cwik, T. A., and Mittra, R. (1987) "Scattering from a periodic array of free-standing arbitrary shaped perfectly conducting or resistive patches," *IEEE Transactions on Antennas Propagation*, vol. 35, no. 11, Nov.

Durschlag, M. S. and DeTemple, T. A. (1981) "Far-IR optical properties of freestanding and dielectrically backed metal meshes," *Applications of Optics*, vol. 20, no. 7, pp. 1245-1253, Apr.

Harrington, R. F. (2000) "The method of moments – a personal review," *Antennas and Propagation Society International Symposium*, vol. 3, pp. 1639-1640, 16-21 July.

Harrington, R. F. (2001) *Time-Harmonic Electromagnetic Fields, A Classical Reissue*, John Wiley & Sons, Inc., New York, pp. 129-131.

Horwitz, C. M. (1974) "A new solar selective surface," *Optical Communications*, vol. 11, no. 2, pp. 210-212, Jun.

Hung, Shih-Che (2005) "Numerical study of frequency selective surfaces by spectral Galerkin Method," Master dissertation, Institute of Applied Mechnics, National Taiwan Unervisity.

Lu, Chang-Tsan (2004) "Analysis of frequency selective surfaces by spectral Galerkin Method," Master dissertation, Institute of Applied Mechnics, National Taiwan Unervisity.

Mittra, R., Chan, C. H. and Cwik, T. (1988) "Techniques for analyzing frequency selective surfaces – A review." *IEEE Proceedings*, vol. 76 (12), pp. 1593-1615, Dec.

Monorchio, A., Manara, G. and Lanuzza, L. (2002) “Synthesis of artificial magnetic conductors by using multilayered frequency selective surfaces,” *IEEE Antennas and Wireless Propagation Letters*, vol. 1, pp. 196-199.

Monorchio, A., Manara, G. and Lanuzza, L. (2003) “Design of high-impedance screens by using multilayered frequency selective surfaces,” *IEEE Antennas and Propagation Society International Symposium*, vol. 2, pp. 415-418.

Rao, Nannapaneni Narayana (2004) “Transmission lines for communications,” *in Elements of Engineering Electromagnetics, Pearson Prentice Hall, pearson Education, Inc*, pp. 439-462.

Rubin, B. J. and Bertoni, H. L. (1983) “Reflection from periodically perforated plane using a subsectional current approximation,” *IEEE Transactions on Antennas Propagations*, vol. 31, no. 6, pp. 829-836, Nov.

Schimert, T., Koch, M. E. and Chan, C. H. (1990) “Analysis of scattering from frequency selective surfaces in the infrared,” *Journal of Optical Society of America*, vol. 7, no. 8, pp. 1545-1553, Aug.

Tsao, C. H. and Mittra, R. (1984) “Spectral-domain analysis of frequency selective surfaces comprised of periodic arrays of cross dipoles and Jerusalem crosses,” *IEEE Transactions on Antennas Propagation*, vol. 32, no. 5, pp. 478-486, May.

Ulrich, R. (1967) “Far-infrared properties of metallic mesh and its complementary structure,” *Infrared Physics*, vol. 7, pp. 37-55.

Wu, T. K. (1995) “Fundamentals of periodic structures,” in *Frequency Selective Surface and Grid Array, Wiley Series in Microwave and Optical Engineering*, Wu T. K. Ed., John Wiley & Sons, Inc, New York, pp. 1-21.